International Journal of Control, Automation, and Systems 21(4) (2023) 1210-1221
http://dx.doi.org/10.1007/s12555-022-0123-7
ISSN:1598-6446 eISSN:2005-4092
http://www.springer.com/12555

Anti-swing and Positioning for Double-pendulum Tower Cranes Using Improved Active Disturbance Rejection Controller

Xinyu Kang, Lin Chai*, and Huikang Liu

Abstract: In most working scenarios of tower cranes, the load swings around the hooks, resulting in a double-pendulum effect. This makes the tower crane more underactuated and nonlinear, and thus more difficult to control. To solve these problems, we design an improved Active Disturbance Rejection Controller (I-ADRC). First, we propose a smooth and non-linear function to reduce the high-frequency oscillation of the system at steady-state and avoid the "chattering" phenomenon. Second, we construct a new type of Extended State Observer (ESO) to improve the dynamic response performance of the system. Then we prove that the closed-loop system is asymptotically stable under reasonable parameters by using the Hurwitz criterion and Lyapunov technique. Numerical simulation results show that our proposed controller has superior control performance and strong robustness.

Keywords: Anti-swing, double-pendulum effect, I-ADRC, positioning, tower cranes.

1. INTRODUCTION

Tower crane, as widely used transportation equipment in ports, construction sites, factories, etc, is being developed towards intelligence and full automation. In the working process of tower crane, the load will swing due to trolley/jib accelerates and decelerates movement or the interference of external forces. As yet, tower cranes are manually operated and usually static or reverse-driven to eliminate load swing, which affects efficiency and is prone to human injury accidents. In many cases: 1) When the hook and the load quality are similar or the hook quality is too heavy to be ignored; 2) When the load quality is not uniform and the size is too large to be regarded as a particle, there will be double-pendulum effect between the load and the hook [1]. That is, the load will swing around the hook with lesser independent inputs than the degrees of freedom, and the system has higher coupling, which brings great challenges to the design of rapid positioning and anti-swing control method of the system.

As a typical crane, tower crane has the advantages of underactuated system, that is, low power consumption and simple mechanical structure. In recent years, the design of tower crane controllers has been studied deeply by many scholars. The various types of existing control methods can be divided into open-loop methods and closed-loop methods according to whether there is closed-loop state feedback in the proposed methods. Input shaping [2-4] and trajectory tracking control [5,6] based on optimal velocity are widely utilised in practical production as easy-to-implement open-loop control strategies. Closed-loop methods such as Lyapunov-based energy analysis methods [7,8], model predictive control (MPC) [9-12], adaptive control [13-17], sliding mode control [18-21], fuzzy control methods [22,23], observer-based methods [24], intelligent control [25-27], and so forth. However, the aforementioned methods ignore an inevitable rope length between the hook and the load, therefore, the quality of the hook is disregarded. Compared with the single-pendulum crane, the double-pendulum effect crane is closer to the actual condition, i.e., the load will rotate irregularly around the hook. So it is challenging to design controller for tower crane with double-pendulum effect.

Tower cranes with double-pendulum effect are mechanical systems with complex dynamics characteristics, and few effective control methods have been proposed. Zhang *et al*. first established the dynamic model of tower cranes with double-pendulum effect [1]. After analyzing and validating the model, then designed an energy-based controller. Moreover, the effectiveness and correctness of the proposed controller were verified by simulations. Ouyang *et al*. designed a controller using energy-shaping-based, which ensures actuator output is physically constrained [28]. A partial enhanced-coupling nonlinear controller is proposed by Tian, to avoid the model uncertainties and external disturbances affecting controller performance [29].

Manuscript received February 10, 2022; revised May 3, 2022; accepted June 5, 2022. Recommended by Associate Editor Ze Tang under the direction of Senior Editor Jessie (Ju H.) Park. This work was supported by the National Key Research and Development Program of China under Grant grant number 2017YFC0805100.

Xinyu Kang, Lin Chai, and Huikang Liu are with the College of Information Science and Engineering, Wuhan University of Science and Technology, Wuhan Hubei 430081, China (e-mails: kaesarxy@163.com, 235126698@qq.com, liuhuikang@wust.edu.cn).
* Corresponding author.

In case of model parameters uncertained, Ouyang *et al*. proposed an adaptive tracking controller to address the influence of non-zero initial swing angles and external disturbances on system [30]. Through numerous simulations, the controller shows good performance. Neural Network (NN) has excellent nonlinear control ability and robust characteristics when solving models with unknown parameters [31], Zhang *et al*. presented an adaptive neural network tracking control method, which controls the trolley and jib quickly track their predetermined trajectories [32]. The controller was compared with other controllers and brought out robustness regarding uncertain model dynamics. Ouyang *et al*. introduced a controller to increase the coupling of actuated and underactuated parts with a simple structure, it also ensures the positioning and anti-swing performance when initial output of actuators is zero. Various experimental results are implemented to validate the control effectiveness [33].

After analyzing and comparing a large number of literature sources, this paper identifies the following problems that need to be solved by existing research.

1) Most of the research regards the tower crane double-pendulum as two-dimensional motion or focuses on a simple single-pendulum, and there are few researches on the three-dimensional complex model of the double-pendulum effect.
2) Despite the above methods can control the positioning of the trolley and jib, the swing angle at all levels can be further reduced.
3) Open-loop control methods such as trajectory tracking and input shaping can achieve control objectives and are widely used, but such methods without state feedback are difficult to deal with unknown disturbances.
4) The influence of "chattering" caused by design defects or external disturbances on the steady-state performance of the system has been ignored in most existing researches.

To this end, the main contributions of this paper are as follows:

1) Based on the ADRC, the designed controller achieves both jib/trolley positioning and rejection of double-pendulum swing angels, meanwhile, a function with nonlinear and smooth characteristics is designed to avoid "chattering".
2) After analysis and a series of comparative simulations, it is verified that the proposed controller has superior robustness concerning model parameters uncertained and significant control performance.

2. TOWER CRANE DYNAMIC MODEL AND CONTROL OBJECTIVE

2.1. Tower crane dyamic model

The structure diagram of the tower crane with underactuated double-pendulum effect is shown in Fig. 1. By using the Lagrange's kinematics equation, the dynamic model is described as follows [1]:

$$
\begin{aligned}
&(J_0 + m_1x^2 + m_2x^2 + M_tx^2 + m_1l_1^2 + m_2l_1^2 + m_2l_2^2 \\
&\quad + 2m_1l_1xC_2S_1 + 2m_2l_1xC_2S_1 + 2m_2l_2xC_4S_3 \\
&\quad + 2m_2l_1l_2S_2S_4 + 2m_2l_1l_2C_2C_4S_1S_3 - m_1l_1^2C_1^2C_2^2 \\
&\quad - m_2l_1^2C_1^2C_2^2 - m_2l_2^2C_3^2C_4^2)\ddot{\alpha} - (m_1l_1S_2 \\
&\quad + m_2l_1S_2 + m_2l_2S_4)\ddot{x} - (m_1l_1^2C_1C_2S_2 + m_2l_1^2C_1C_2S_2 \\
&\quad + m_2l_1l_2C_1C_2S_4)\ddot{\theta}_1 + (m_1l_1^2S_1 + m_2l_1^2S_1 \\
&\quad + m_1l_1xC_2 + m_2l_1xC_2 + m_2l_1l_2C_2C_4S_3 \\
&\quad + m_2l_1l_2S_1S_2S_4)\ddot{\theta}_2 - (m_2l_2^2C_3C_4S_4 \\
&\quad + m_2l_1l_2C_3C_4S_2)\ddot{\theta}_3 + (m_2l_2^2S_3 + m_2l_2xC_4 \\
&\quad + m_2l_1l_2C_2C_4S_1 + m_2l_1l_2S_2S_3S_4)\ddot{\theta}_4 \\
&\quad + 2m_1x\dot{\alpha}\dot{x} + 2m_2x\dot{\alpha}\dot{x} + 2M_tx\dot{\alpha}\dot{x} + 2\dot{\alpha}\dot{x}m_1l_1C_2S_1 \\
&\quad + 2m_2l_1C_2S_1\dot{\alpha}\dot{x} \\
&\quad + 2m_2l_2C_4S_3\dot{\alpha}\dot{x} + 2m_1l_1^2C_1C_2^2S_1\dot{\theta}_1\dot{\alpha} \\
&\quad + 2m_2l_1^2C_1C_2^2S_1\dot{\theta}_1\dot{\alpha} + 2m_2l_1xC_1C_2\dot{\theta}_1\dot{\alpha}
\end{aligned}
$$

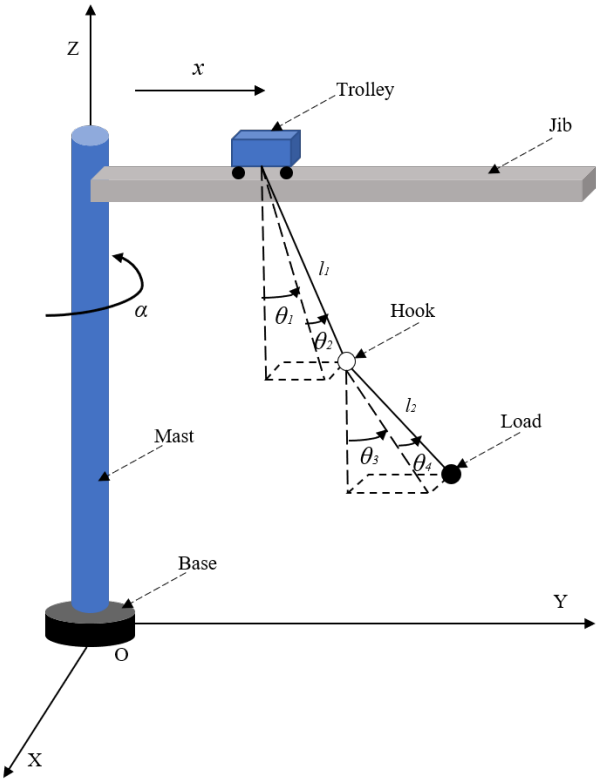

Fig. 1. Tower crane model.

$$
\begin{aligned}
&+2m_1l_1xC_1C_2\dot{\theta}_1\dot{\alpha}+2m_1l_1^2C_1\dot{\theta}_1\dot{\theta}_2\\
&+2m_2l_1l_2C_1C_2C_4S_3\dot{\theta}_1\dot{\alpha}+2m_1l_1^2C_1^2C_2S_2\dot{\theta}_2\dot{\alpha}\\
&+2m_2l_1^2C_1^2C_2S_2\dot{\theta}_2\dot{\alpha}+2m_2l_1l_2C_2S_4\dot{\theta}_2\dot{\alpha}\\
&-2m_2l_1xS_1S_2\dot{\theta}_2\dot{\alpha}-2m_1l_1xS_1S_2\dot{\theta}_2\dot{\alpha}\\
&-2m_2l_1l_2C_4S_1S_2S_3\dot{\theta}_2\dot{\alpha}+2m_2l_2^2C_3C_4^2S_3\dot{\theta}_3\dot{\alpha}\\
&+2m_2l_2xC_3C_4\dot{\theta}_3\dot{\alpha}+2m_2l_1l_2C_2C_3C_4S_1\dot{\theta}_3\dot{\alpha}\\
&+2m_2l_2^2C_3^2C_4S_4\dot{\theta}_4\dot{\alpha}-m_2l_2xS_4\dot{\theta}_4^2\\
&+2m_2l_1l_2C_4S_2\dot{\theta}_4\dot{\alpha}-2m_2l_2xS_3S_4\dot{\theta}_4\dot{\alpha}\\
&-2m_2l_1l_2C_2S_1S_3S_4\dot{\theta}_4\dot{\alpha}+m_1l_1^2C_2S_1S_2\dot{\theta}_1^2\\
&+m_2l_1^2C_2S_1S_2\dot{\theta}_1^2+m_2l_1l_2C_2S_1S_4\dot{\theta}_1^2\\
&+2m_2l_1^2C_1\dot{\theta}_1\dot{\theta}_2+2m_2l_1l_2C_1S_2S_4\dot{\theta}_1\dot{\theta}_2\\
&-2m_1l_1^2C_1C_2^2\dot{\theta}_1\dot{\theta}_2-2m_2l_1^2C_1C_2^2\dot{\theta}_1\dot{\theta}_2\\
&+m_2l_1l_2C_2S_1S_4\dot{\theta}_2^2-m_2l_1l_2C_4S_2S_3\dot{\theta}_2^2\\
&-m_1l_1xS_2\dot{\theta}_2^2-m_2l_1xS_2\dot{\theta}_2^2\\
&+m_2l_2^2C_4S_3S_4\dot{\theta}_3^2+m_2l_1l_2C_4S_2S_3\dot{\theta}_3^2+2m_2l_2^2C_3\dot{\theta}_3\dot{\theta}_4\\
&-2m_2l_2^2C_3C_4^2\dot{\theta}_3\dot{\theta}_4+2m_2l_1l_2C_3S_2S_4\dot{\theta}_3\dot{\theta}_4\\
&-m_2l_1l_2C_2S_1S_4\dot{\theta}_4^2+m_2l_1l_2C_4S_2S_3\dot{\theta}_4^2=T_a-T_f,
\end{aligned}
\tag{1}
$$

$$
\begin{aligned}
&-(m_1l_1S_2+m_2l_1S_2+m_2l_2S_4)\ddot{\alpha}+(M_t+m_1+m_2)\ddot{x}\\
&+(m_1l_1C_1C_2+m_2l_1C_1C_2)\ddot{\theta}_1\\
&-(m_1l_1S_1S_2+m_2l_1S_1S_2)\ddot{\theta}_2+m_2l_2C_3C_4\ddot{\theta}_3\\
&-m_2l_2S_3S_4\ddot{\theta}_4-m_1x\dot{\alpha}^2-m_2x\dot{\alpha}^2-M_tx\dot{\alpha}^2\\
&-m_1l_1C_2S_1\dot{\alpha}^2-m_2l_1C_2S_1\dot{\alpha}^2\\
&-m_2l_2C_4S_3\dot{\alpha}^2-2m_1l_1C_2\dot{\theta}_2\dot{\alpha}-2m_2l_1C_2\dot{\theta}_2\dot{\alpha}\\
&-2m_2l_2C_4\dot{\theta}_4\dot{\alpha}-m_1l_1C_2S_1\dot{\theta}_1^2\\
&-m_2l_1C_2S_1\dot{\theta}_1^2-2m_1l_1C_1S_2\dot{\theta}_1\dot{\theta}_2-2m_2l_1C_1S_2\dot{\theta}_1\dot{\theta}_2\\
&-m_1l_1C_2S_1\dot{\theta}_2^2-m_2l_1C_2S_1\dot{\theta}_2^2\\
&-m_2l_2C_4S_3\dot{\theta}_3^2-2m_2l_2C_3S_4\dot{\theta}_3\dot{\theta}_4\\
&-m_2l_2C_4S_3\dot{\theta}_4^2=F_x-F_f,
\end{aligned}
\tag{2}
$$

$$
\begin{aligned}
&-(m_2l_1^2C_1C_2S_2+l_1m_2l_2C_1C_2S_4+m_1l_1^2C_1C_2S_2)\ddot{\alpha}\\
&+(m_1l_1C_1C_2+m_2l_1C_1C_2)\ddot{x}+(m_1l_1^2C_2^2+m_2l_1^2C_2^2)\ddot{\theta}_1\\
&+(m_2l_1l_2C_1C_2C_3C_4+m_2l_1l_2C_2C_4S_1S_3)\ddot{\theta}_3\\
&+(m_2l_1l_2C_2C_3S_1S_4-m_2l_1l_2C_1C_2S_3S_4)\ddot{\theta}_4\\
&-m_1l_1^2C_1C_2^2S_1\dot{\alpha}^2-2m_2l_1l_2C_1C_2C_3S_4\dot{\theta}_3\dot{\theta}_4\\
&-m_1l_1xC_1C_2\dot{\alpha}^2-m_2l_1xC_1C_2\dot{\alpha}^2\\
&-m_2l_1l_2C_1C_2C_4S_3\dot{\alpha}^2\\
&-2m_1l_1^2C_1C_2^2\dot{\theta}_2\dot{\alpha}-2m_2l_1^2C_1C_2^2\dot{\theta}_2\dot{\alpha}\\
&-2m_2l_1l_2C_1C_2C_4\dot{\theta}_4\dot{\alpha}-2m_1l_1^2C_2S_2\dot{\theta}_1\dot{\theta}_2\\
&-2m_2l_1^2C_2S_2\dot{\theta}_1\dot{\theta}_2-m_2l_1l_2C_1C_2C_4S_3\dot{\theta}_3^2\\
&+m_2l_1l_2C_2C_3C_4S_1\dot{\theta}_3^2-m_2l_1^2C_1C_2^2S_1\dot{\alpha}^2\\
&-2m_2l_1l_2C_2S_1S_3S_4\dot{\theta}_3\dot{\theta}_4-m_2l_1l_2C_1C_2C_4S_3\dot{\theta}_4^2\\
&+m_2l_1l_2C_2C_3C_4S_1\dot{\theta}_4^2\\
&+(m_1+m_2)gl_1C_2S_1=0,
\end{aligned}
\tag{3}
$$

$$
\begin{aligned}
&(m_1l_1^2S_1+m_2l_1^2S_1+m_1l_1xC_2+m_2l_1xC_2\\
&+m_2l_1l_2C_2C_4S_3\\
&+m_2l_1l_2S_1S_2S_4)\ddot{\alpha}-(m_1l_1S_1S_2+m_2l_1S_1S_2)\ddot{x}\\
&+(m_2l_1l_2C_1C_4S_2S_3-m_2l_1l_2C_3C_4S_1S_2)\ddot{\theta}_3\\
&+(m_1l_1^2+m_2l_1^2)\ddot{\theta}_2+(m_2l_1l_2C_1C_3S_2S_4\\
&+m_2l_1l_2S_1S_2S_3S_4+m_2l_1l_2C_2C_4)\ddot{\theta}_4+2m_1l_1C_2\dot{\alpha}\dot{x}\\
&-m_1l_1^2C_1^2C_2S_2\dot{\alpha}^2-m_2l_1^2C_1^2C_2S_2\dot{\alpha}^2-l_1m_2l_2C_2S_4\dot{\alpha}^2\\
&+m_2l_1xS_1S_2\dot{\alpha}^2+m_2l_1l_2C_4S_1S_2S_3\dot{\alpha}^2+m_1l_1xS_1S_2\dot{\alpha}^2\\
&+2m_2l_1C_2\dot{\alpha}\dot{x}+2m_1l_1^2C_1C_2^2\dot{\theta}_1\dot{\alpha}+2m_2l_1^2C_1C_2^2\dot{\theta}_1\dot{\alpha}\\
&+2m_2l_1l_2C_2C_3C_4\dot{\theta}_3\dot{\alpha}+2m_2l_1l_2C_4S_1S_2\dot{\theta}_4\dot{\alpha}\\
&-2m_2l_1l_2C_2S_3S_4\dot{\theta}_4\dot{\alpha}+m_1l_1^2C_2S_2\dot{\theta}_1^2\\
&+m_2l_1^2C_2S_2\dot{\theta}_1^2+m_2l_1l_2C_1C_3C_4S_2\dot{\theta}_3^2\\
&+m_2l_1l_2C_4S_1S_2S_3\dot{\theta}_3^2-2m_2l_1l_2C_1S_2S_3S_4\dot{\theta}_3\dot{\theta}_4\\
&+2m_2l_1l_2C_3S_1S_2S_4\dot{\theta}_3\dot{\theta}_4-m_2l_1l_2C_2S_4\dot{\theta}_4^2\\
&+m_2l_1l_2C_1C_3C_4S_2\dot{\theta}_4^2+m_2l_1l_2C_4S_1S_2S_3\dot{\theta}_4^2\\
&+(m_1+m_2)gl_1C_1S_2=0,
\end{aligned}
\tag{4}
$$

$$
\begin{aligned}
&-(m_2l_2^2C_3C_4S_4+m_2l_1l_2C_3C_4S_2)\ddot{\alpha}+m_2l_2C_3C_4\ddot{x}\\
&+(m_2l_1l_2C_1C_2C_3C_4+m_2l_1l_2C_2C_4S_1S_3)\ddot{\theta}_1\\
&+(m_2l_1l_2C_1C_4S_2S_3-m_2l_1l_2C_3C_4S_1S_2\ddot{\theta}_2\\
&+m_2l_2^2C_4^2\ddot{\theta}_3-m_2l_2^2C_3C_4^2S_3\dot{\alpha}^2-m_2l_2xC_3C_4\dot{\alpha}^2\\
&-m_2l_1l_2C_2C_3C_4S_1\dot{\alpha}^2-2m_2l_1l_2C_2C_3C_4\dot{\theta}_2\dot{\alpha}\\
&-2m_2l_2^2C_3C_4^2\dot{\theta}_4\dot{\alpha}+m_2l_1l_2C_1C_2C_4S_3\dot{\theta}_1^2\\
&-m_2l_1l_2C_2C_3C_4S_1\dot{\theta}_1^2-2m_2l_1l_2C_1C_3C_4S_2\dot{\theta}_1\dot{\theta}_2\\
&-2m_2l_1l_2C_4S_1S_2S_3\dot{\theta}_1\dot{\theta}_2+m_2l_1l_2C_1C_2C_4S_3\dot{\theta}_2^2\\
&-m_2l_1l_2C_2C_3C_4S_1\dot{\theta}_2^2-2m_2l_2^2C_4S_4\dot{\theta}_3\dot{\theta}_4\\
&+gm_2l_2C_4S_3=0,
\end{aligned}
\tag{5}
$$

$$
\begin{aligned}
&(m_2l_2^2S_3+m_2l_2xC_4+m_2l_1l_2C_2C_4S_1+m_2l_1l_2S_2S_3S_4)\ddot{\alpha}\\
&-m_2l_2S_3S_4\ddot{x}+(m_2l_1l_2C_2C_3S_1S_4\\
&-m_2l_1l_2C_1C_2S_3S_4)\ddot{\theta}_1\\
&+(m_2l_1l_2C_2C_4+m_2l_1l_2C_1C_3S_2S_4\\
&+m_2l_1l_2S_1S_2S_3S_4)\ddot{\theta}_2\\
&+m_2l_2^2\ddot{\theta}_4-m_2l_2^2C_3^2C_4S_4\dot{\alpha}^2-m_2l_1l_2C_4S_2\dot{\alpha}^2\\
&+m_2l_2xS_3S_4\dot{\alpha}^2+m_2l_1l_2C_2S_1S_3S_4\dot{\alpha}^2+2m_2l_2C_4\dot{\alpha}\dot{x}\\
&+2m_2l_1l_2C_1C_2C_4\dot{\theta}_1\dot{\alpha}-2m_2l_1l_2C_4S_1S_2\dot{\theta}_2\dot{\alpha}\\
&+2m_2l_1l_2C_2S_3S_4\dot{\theta}_2\dot{\alpha}+2m_2l_2^2C_3C_4^2\dot{\theta}_3\dot{\alpha}\\
&+m_2l_1l_2C_1C_2C_3S_4\dot{\theta}_1^2+m_2l_1l_2C_2S_1S_3S_4\dot{\theta}_1^2\\
&+2m_2l_1l_2C_1S_2S_3S_4\dot{\theta}_1\dot{\theta}_2-2m_2l_1l_2C_3S_1S_2S_4\dot{\theta}_1\dot{\theta}_2\\
&-m_2l_1l_2C_4S_2\dot{\theta}_2^2+m_2l_1l_2C_1C_2C_3S_4\dot{\theta}_2^2\\
&+m_2l_1l_2C_2S_1S_3S_4\dot{\theta}_2^2+m_2l_2^2C_4S_4\dot{\theta}_3^2
\end{aligned}
$$

$$+ gm_2 l_2 C_3 S_4 = 0, \tag{6}$$

where M_t, m_1, m_2 represent the trolley mass, the hook mass, the load mass, respectively. θ_1 and θ_3 are the angles of the hook and load in the plane of the mast and jib, respectively. θ_2 and θ_4 are the angles of the hook and load out of that plane, respectively. The length of the rope and rigging are represented as l_1 and l_2, respectively. The moment of inertia of the jib is denoted as j_0, and g is the gravitational acceleration. α represents the jib slew angle, and x is the trolley displacement. T_α denotes the slew driving torque, F_x is the trolley motion driving force, and T_f, F_f are the friction torque and force, respectively.

$$T_f = f_{11} \tanh\left(\frac{\dot{\alpha}}{\varepsilon_1}\right) + f_{12}|\dot{\alpha}|\dot{\alpha}, \tag{7}$$

$$F_f = f_{21} \tanh\left(\frac{\dot{x}}{\varepsilon_2}\right) + f_{22}|\dot{x}|\dot{x}. \tag{8}$$

The friction model can be derived as follows by using friction compensation [28,29]: f_{11}, f_{12}, f_{21}, f_{22}, ε are the friction-related parameters, which are 5.2, 0.6, 4.4, 0.5 and 0.01 after offline experiments and data fitting, respectively.

In order to keep generality and facilitate controller design and stability analysis, the tower crane system often has the following assumptions:

1) The mass of the rope and rigging is ignored and considered as a rigid link, then their deformation and twist and other non-linear factors can be regardless.
2) In the practice case, the load cannot exceed the jib , and load usually swings below the hook, that is, the values of swing angles are limited θ_1, θ_2, θ_3, $\theta_4 \in \left(-\frac{\pi}{2}, \frac{\pi}{2}\right)$.
3) When the state of the tower crane is close to the equilibrium point, the hook and load swing angles (θ_i, $i = 1, 2, 3, 4$) are very small, therefore, $cos\theta_i = 1$ and $sin\theta_i = 0$ are reasonable, $\dot{\theta}_i\dot{\theta}_j = \dot{\theta}_i^2 = 0 (i \neq j, j = 1,2,3,4)$,and $\dot{\alpha}\dot{x} = \dot{\alpha}^2 = \dot{x}^2 = 0$ are also logical.

2.2. Control objective

The control objective of the tower crane is to quickly transport the load from the initial position to the desired position. At the same time, minimizing the swing angle as much as possible and eliminating residual swing angles. Therefore, the control shall achieve the following objectives:

1) The jib/trolley must reach the desired position, and the mathematical expression is as follows:

$$\lim_{t\to\infty} \alpha = \alpha_d, \lim_{t\to\infty} x = x_d, \tag{9}$$

where α_d and x_d are the positions planned for jib and trolley.

2) The swing angles of hook and load must also be restrained during positioning, and the expressions are as follows:

$$\lim_{t\to\infty} \theta_1 = 0, \lim_{t\to\infty} \theta_2 = 0, \lim_{t\to\infty} \theta_3 = 0, \lim_{t\to\infty} \theta_4 = 0. \tag{10}$$

3. CONTROLLER DESIGN AND STABILITY ANALYSIS

In this section, to achieve suppress the swing angles of the double-pendulum effect, and eliminate "chattering" on the system output, while accurately positioning the jib/trolley. An improved Active Disturbance Rejection Controller (I-ADRC) will be proposed. Then, the stability of the closed-loop controller is proved by Hurwitz Criterion and Lyapunov technique.

ADRC is a nonlinear controller independent of parameters certained model. Its idea is to synthesize the internal and external disturbances of the system into a "total disturbance" to compensate for the feedback loop. ADRC does not require a prior model of directly measured external disturbances and has excellent disturbances resistance and robustness [27,34].

Based on the theory of linearization and decoupling, a simplified model is derived in this paper [35]. The model is presented as follows for the purpose of facilitating the controller design and system

$$(J_0 + M_t x_d^2 + m_1 x_d^2 + m_2 x_d^2)\ddot{\alpha} + (m_1 + m_2) l_1 x_d \ddot{\theta}_2 + m_2 l_2 x_d \ddot{\theta}_4 = T_a, \tag{11}$$

$$(M_t + m_1 + m_2)\ddot{x} + (m_1 + m_2) l_1 \ddot{\theta}_1 + m_2 l_2 \ddot{\theta}_3 = F_x, \tag{12}$$

$$(m_1 + m_2) l_1 \ddot{x} + (m_1 + m_2) l_1^2 \ddot{\theta}_1 + m_2 l_1 l_2 \ddot{\theta}_3 + (m_1 + m_2) g l_1 \theta_1 = 0, \tag{13}$$

$$(m_1 + m_2) l_1 x_d \ddot{\alpha} + (m_1 + m_2) l_1^2 \ddot{\theta}_2 + m_2 l_1 l_2 \ddot{\theta}_4 + (m_1 + m_2) g l_1 \theta_2 = 0, \tag{14}$$

$$m_2 l_2 \ddot{x} + m_2 l_1 l_2 \ddot{\theta}_1 + m_2 l_2^2 \ddot{\theta}_3 + m_2 g l_2 \theta_3 = 0, \tag{15}$$

$$m_2 l_2 x_d \ddot{\alpha} + m_2 l_1 l_2 \ddot{\theta}_2 + m_2 l_2^2 \ddot{\theta}_4 + m_2 g l_2 \theta_4 = 0. \tag{16}$$

The dynamic model can also be changed into

$$\begin{cases} \dot{\boldsymbol{q}}_2 = [\boldsymbol{f(t)} + \boldsymbol{w(t)}] + \boldsymbol{b U_a}, \\ \dot{\boldsymbol{q}}_1 = \boldsymbol{q_2}, \end{cases} \tag{17}$$

where $\boldsymbol{U_a}$ represent system inputs; $\boldsymbol{q_1}$ represent state variables; $\boldsymbol{b}$ is the control signal gain coefficient; the $\boldsymbol{f(t)} + \boldsymbol{w(t)}$ were related to the system state, the unknown external disturbance represents real-time action, and its derivatives are classified as the "total disturbance". They are explicitly included in Appendix A.

3.1. Controller design

The designed tower crane with double-pendulum effect controller (ADRC) consists of three modules: tracking dif-

ferentiator (TD), improved nonlinear state error feedback control rate (NLSEF), and improved extended state observer (ESO). This subsection describes the design of the controller for the trolley luffing subsystem of the tower crane.

3.1.1 Tracking differentiator

The TD is utilised to arrange the input signal transition process and smooth the signal to avoid excessive overshoot caused by the large difference between the given value and the actual feedback value. Its discrete form can be expressed as

$$\begin{cases} u(k) = fhan\left(x_1(k) - v(k), x_2(k), r_1, h_0\right), \\ x_1(k+1) = x_1(k) + h_1 x_2(k), \\ x_2(k+1) = x_2(k) + h_1 u(k). \end{cases} \tag{18}$$

In the formula, $fhan(x_1, x_2, r_1, h_0)$ is the fastest comprehensive function, which is utilised to fast track the input of the target value, and its formula can be expressed as

$$\begin{cases} d = r_1 {h_0}^2, \\ j_0 = h_0 x_2(k), \\ y = x_1(k) + j_0, \\ j_1 = \sqrt{d(d + 8|y|)}, \\ j_2 = j_0 + sign(y)\left(j_1 - d\right)/2, \\ j = (j_0 + y)\, fsg(v,d) + j_2(1 - fsg(y,d)), \\ fhan = -r\left(\dfrac{j}{d}\right) fsg(j,d) \\ \qquad\qquad - r \cdot sign(j)(1 - fsg(j,d)). \end{cases} \tag{19}$$

The $fsg(j,d)$ for eliminating high frequency signals is defined as

$$fsg(j,d) = (sign(j+d) - sign(j-d))/2, \tag{20}$$

where h is the sampling period; r is the rate factor of the tracking input signal; $h_0 = n * h$, n is an integer between 1 and 20, and h_0 determines the ability of the controller to eliminate the noise component in the tracking signal.

3.1.2 Improved nonlinear state error feedback control rate

NLSEF transforms the control law of system with unknown external disturbances into a PI series-type process using a nonlinear function.

The NLSEF and ESO in traditional ADRC use a nonlinear piecewise $fal(e, \gamma, \delta)$ to eliminate high frequency "chattering" near the error zero. Among them, e is the error signal; γ is the given nonlinear factor; δ determines the interval span of the nonlinear segment.

However, after analysis, it is found that $fal(e, \gamma, \delta)$ is continuous but not smooth near the $\pm\delta$. In order to avoid the "chattering" of the system due to $fal(e, \gamma, \delta)$, a $kas(e, \gamma, \delta)$ with better global smoothness is designed to improve controller steady-state accuracy and performance.When the jib/trolley is controlled near the control target, the tracking error hovers around zero, and the $kas(e, \gamma, \delta)$ is the judgment condition for the magnitude of the error. $kas(e, \gamma, \delta)$ is fitted by a linear segment and a sinusoidal segment, during $|e| \le \delta$ the $kas(e, \gamma, \delta)$ can be expressed as

$$kas(e, \gamma, \delta) = G_1 e + G_2 e^2 + G_3 \sin e. \tag{21}$$

When $|e| \le \delta$, it is consistent with the $fal(e, \gamma, \delta)$, then,gain functions G_1, G_2, and G_3 can be calculated by ensuring that the piecewise function satisfies the boundary condition and is smooth and continuous when $|e| = \delta$. Finally, the complete $kas(e, \gamma, \delta)$ can be represented as

$$kas(e, \gamma, \delta) = \begin{cases} (a\delta^{\gamma-1} - \dfrac{(1-\gamma)\delta^{\gamma}\cos\delta}{\sin\delta - \delta\cos\delta})e \\ \quad + \dfrac{(1-\gamma)\delta^{\gamma}}{\sin\delta - \delta\cos\delta}\sin e, \ |e| \le \delta, \\ |e|^{\gamma} sign(e), \ |e| > \delta. \end{cases} \tag{22}$$

In order to verify the improvement of the $kas(e, \gamma, \delta)$ function compared to the $fal(e, \gamma, \delta)$ function, Fig. 2 shows the respective response of them at $\delta = 0.1$; $\gamma = 0$, 0.25, 0.5, 0.75 and the comparison response at $\delta = 0.1$; $\gamma = 0.25$. It can be clearly seen from the comparison results that, compared with $fal(e, \gamma, \delta)$, $kas(e, \gamma, \delta)$ not only has global smoothness throughout the entire interval but also has better continuity. By using $kas(e, \gamma, \delta)$, the "chattering" caused by the traditional function with high frequency switching to the state variables of the system at all levels can be effectively avoided. Furthermore, the performance of the controller is correspondingly improved.

Then the improved discrete form of NLSEF is as follows:

$$\begin{cases} e_1(k) = v_{11}(k) - z_1(k), e_2(k) = v_{12}(k) - z_2(k), \\ e_{3(k)} = v_{21}(k) - v_{31}(k), e_4(k) = v_{22}(k) - v_{32}(k), \\ e_5(k) = v_{41}(k) - v_{51}(k), e_6(k) = v_{42}(k) - v_{52}(k), \\ u_a = k_1 \cdot kas\left(e_1, \gamma_1, \delta_0\right) + k_2 \cdot kas\left(e_2, \gamma_2, \delta_0\right), \\ u_b = k_3 \cdot kas\left(e_3, \gamma_1, \delta_0\right) + k_4 \cdot kas\left(e_4, \gamma_2, \delta_0\right), \\ u_c = k_5 \cdot kas\left(e_5, \gamma_1, \delta_0\right) + k_6 \cdot kas\left(e_6, \gamma_2, \delta_0\right), \\ u_1 = u_a + u_b + u_c, \\ F_x = u_1 - \dfrac{z_3(k)}{b_1}, \end{cases} \tag{23}$$

where $0 < a_1 < 1 < a_2$; k_1, k_3 and k_5 are proportional regulating factors; k_2, k_4 and k_6 are differential regulatory factors; b_1 is the compensation factor; $kas(e, \gamma, \delta)$ is the new nonlinear function; e_i (i = 1, 2, ..., 6) are the state errors of the system; u_1 is the superposition output of three cascaded nonlinear PD control laws.

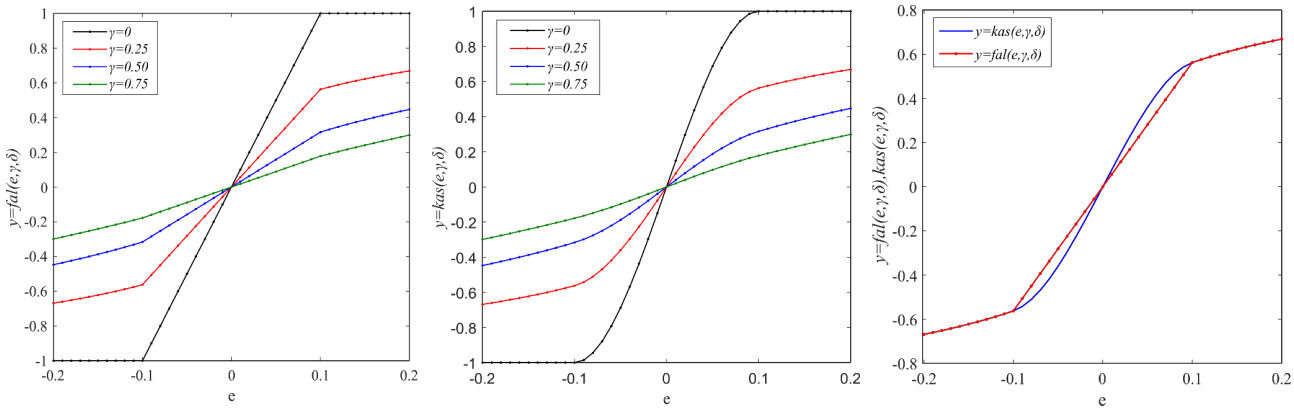

Fig. 2. $fal(e,\gamma,\delta)$ and $kas(e,\gamma,\delta)$ comparison.

3.1.3 Improved extended state observer

ESO uses higher-order state variables to dynamically compensate for real-time estimated total system disturbances. In the classical extended state observer, $z_1(k)$ tracks the system input signal, $z_2(k)$ tracks the differential component of the system output signal, and $z_3(k)$ is the "total disturbances" estimated value. Considering that the trolley variable amplitude displacement x differential dispersion form $x_2(k)$ also has a physical reference in the design process of the controller, $x_2(k)$ should be used as the target variable of the observed value $z_2(k)$. The expression of the designed improved ESO is as follows:

$$\begin{cases} e_1(k) = z_1(k) - x_1(k), e_2(k) = z_2(k) - x_2(k), \\ z_1(k+1) = z_1(k) + h[z_2(k) - \beta_{01} e_1(k)], \\ z_2(k+1) = z_2(k) + h[z_3 - \beta_{02} e_2(k)] + b_1 \cdot F_x, \\ z_3(k+1) = z_3(k) - h[\beta_{03} kas(e_1(k), \gamma_{01}, \delta_1) \\ \qquad + \beta_{04} kas(e_2(k), \gamma_{02}, \delta_1)], \end{cases} \tag{24}$$

where β_{01}, β_{02}, β_{03}, and β_{04} are the gains of the state error feedback, which determine the dynamic performance of the ESO convergence. The four parameters are coupled with each other and play a key role in the stability of the system. $x_1(k)$ is the discrete quantity of the trolley displacement.

The $z_3(k)$ in the improved ESO can more effectively estimate the "total disturbance", which includes changes in model parameters (double-pendulum mass and rope length) and external disturbances, i.e., the disturbances that can affect the output of the system (the swing angles of all levels, the position of trolley and arm), or the disturbances that can be observed by the system output. After $z_3(k)$ is compensated by the error feedback in NLSEF, the robustness of the controller is enhanced.

In order to reduce the difficulty of manual tuning parameters, the concept of observer bandwidth proposed by Gao [36] is utilised in this paper, that is, $\beta_{01} = 3\omega_1$, $\beta_{02} = 3\omega_1^2$, $\beta_{03} = \omega_1^3$, $\beta_{04} = \beta_{03}$, and ω_1 defined as the observer bandwidth.

The rotary controller is exactly the same as the above structure, only the key parameters need to be adjusted again according to the control objective. Hence, the structure schematic diagram of tower crane with double-pendulum effect I-ADRC is shown in Fig. 3.

3.2. Controller stability analysis

In the design of the expansion observer in the above section, all poles of ESO are configured as $-\omega_1$, which satisfies $\omega_1 > 0$, then set up the observer's closed-loop poles to ensure stability, they satisfy the following relation:

$$v(s) = s^3 + 3\omega_1 s^2 + 3\omega_1^2 s + \omega_1^3. \tag{25}$$

According to the dynamic model, let $\xi_1 = x$, $\xi_2 = \dot{x}$, $\xi_3 = \boldsymbol{f_1(t)}$, $\boldsymbol{\xi} = \begin{bmatrix} \xi_1 & \xi_2 & \xi_3 \end{bmatrix}^T$, $\boldsymbol{f_1(t)}$ is the "total disturbances" of the internal and external disturbances of the trolley x displacement system. Assuming $\boldsymbol{f_1(t)}$ is bounded and differentiable, then $\left|\dot{\boldsymbol{f}}_1(t)\right| = \boldsymbol{R} \le s$, and $s > 0$. According to (17). The state vector equation of trolley control subsystem is as follows:

$$\begin{cases} \dot{\boldsymbol{\xi}} = \boldsymbol{A\xi} + \boldsymbol{BU_1} + \boldsymbol{ER}, \\ \boldsymbol{x} = \boldsymbol{C\xi}, \end{cases} \tag{26}$$

where $\boldsymbol{A} = \begin{bmatrix} 0 & 1 & 0 \\ 0 & 0 & 1 \\ 0 & 0 & 0 \end{bmatrix}$, $\boldsymbol{B} = \begin{bmatrix} 0 \\ \dfrac{1}{M_t} \\ 0 \end{bmatrix}$, $\boldsymbol{U_1} = F_x$, $\boldsymbol{C} = \begin{bmatrix} 1 & 0 & 0 \end{bmatrix}$, $\boldsymbol{E} = \begin{bmatrix} 0 & 0 & 1 \end{bmatrix}^T$. And, set $\boldsymbol{D} = \begin{bmatrix} 3\omega_1 & 3\omega_1^2 & \omega_1^3 \end{bmatrix}^T$, then $d_1 = 3\omega_1$, $d_2 = 3\omega_1^2$, $d_3 = \omega_1^3$. Performing simple mathematical operations on (26) gives the following results:

$$\begin{cases} \dot{\widetilde{\boldsymbol{\xi}}}_1 = \widetilde{\boldsymbol{\xi}}_2 - d_1 \widetilde{\boldsymbol{\xi}}_1, \\ \dot{\widetilde{\boldsymbol{\xi}}}_2 = \widetilde{\boldsymbol{\xi}}_3 - d_2 \widetilde{\boldsymbol{\xi}}_1, \\ \dot{\widetilde{\boldsymbol{\xi}}}_3 = \boldsymbol{R} - d_3 (\widetilde{\boldsymbol{\xi}}_1 + \widetilde{\boldsymbol{\xi}}_2). \end{cases} \tag{27}$$

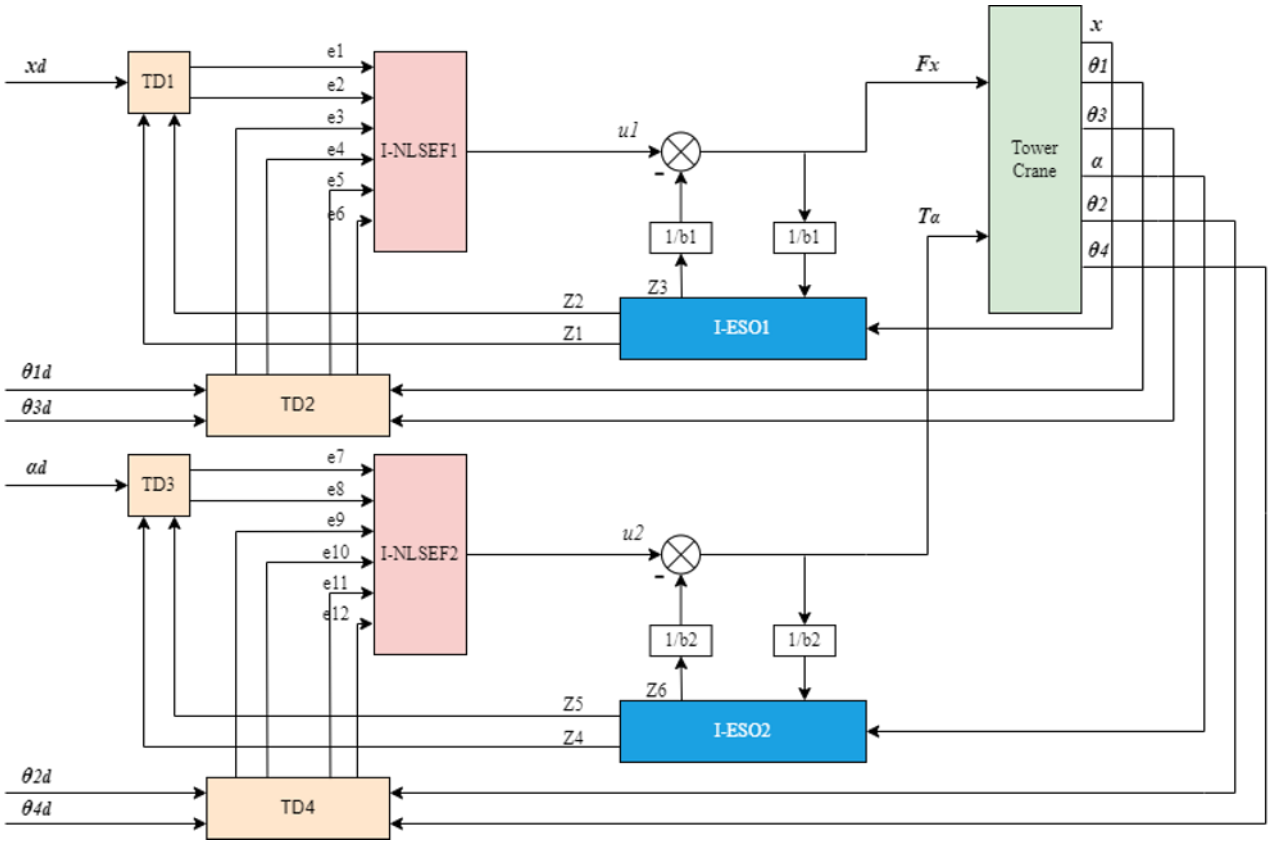

Fig. 3. Control scheme of the tower crane system.

Let $\boldsymbol{\zeta_i} = (\tilde{\xi}_i)/\left(\omega_1^{i-1}\right)(i=1,2,3)$ be as follows:

$$\dot{\boldsymbol{\zeta}} = \omega_1 \boldsymbol{A_\zeta}\boldsymbol{\zeta} + \frac{\boldsymbol{B_\zeta}}{{\omega_1}^2}\boldsymbol{R} \tag{28}$$

where $\boldsymbol{A_\zeta} = \begin{bmatrix} -3 & 1 & 0 \\ -3 & 0 & 1 \\ -1 & -\omega_1 & 0 \end{bmatrix}$ is verified to be a Hurwitz matrix, $\boldsymbol{B_\zeta} = \begin{bmatrix} 0 & 0 & 1 \end{bmatrix}^T$ And $\boldsymbol{A_\zeta}$ should satisfy the following formula:

$${\boldsymbol{A_\zeta}}^T\boldsymbol{P} + \boldsymbol{P}\boldsymbol{A_\zeta} = -\boldsymbol{W}. \tag{29}$$

When $\boldsymbol{W}$ is any positive definite constant and symmetric matrix, then $\boldsymbol{P}$ must exist as a positive definite symmetric matrix, then the system is asymptotically stable.

The following Lyapunov candidate function V is introduced to analyze the stability of the closed-loop system

$$\boldsymbol{V_1} = \tilde{\boldsymbol{\zeta}}^T\boldsymbol{P}\tilde{\boldsymbol{\zeta}}. \tag{30}$$

The derivative of the proposed Lyapunov function V with respect to time is obtained as follows:

$$\begin{aligned}\dot{\boldsymbol{V}}_1 &= \dot{\tilde{\boldsymbol{\zeta}}}^T\boldsymbol{P}\tilde{\boldsymbol{\zeta}} + \tilde{\boldsymbol{\zeta}}^T\boldsymbol{P}\dot{\tilde{\boldsymbol{\zeta}}} \\ &= \frac{1}{\omega_1}\dot{\tilde{\boldsymbol{\zeta}}}^T\left({\boldsymbol{A_\zeta}}^T\boldsymbol{P} + \boldsymbol{P}\boldsymbol{A_\zeta}\right)\tilde{\boldsymbol{\zeta}} + 2\boldsymbol{\zeta}^T\widetilde{\boldsymbol{P}\boldsymbol{B_\zeta}f_1}(t) \\ &\le -\frac{1}{\omega_1}\tilde{\boldsymbol{\zeta}}^T\boldsymbol{W}\tilde{\boldsymbol{\zeta}} + 2\left\|\boldsymbol{P}\boldsymbol{B_\zeta}\right\|\cdot\|\tilde{\boldsymbol{\zeta}}\|\cdot\boldsymbol{R} \\ &\le -\frac{1}{\omega_1}\boldsymbol{\lambda}_{\min}(\boldsymbol{W})\|\tilde{\boldsymbol{\zeta}}\|^2 + 2s\left\|\boldsymbol{P}\boldsymbol{B_\zeta}\right\|\cdot\|\tilde{\boldsymbol{\zeta}}\|,\end{aligned} \tag{31}$$

where $\boldsymbol{\lambda}_{min}(\boldsymbol{W})$ is the minimum eigenvalue in $\boldsymbol{W}$ matrix. If the closed-loop system is Lyapunov asymptotically stable, the following inequalities must be satisfied

$$\|\tilde{\boldsymbol{\zeta}}\| \le \frac{2s\omega_1\left\|\boldsymbol{P}\boldsymbol{B_\zeta}\right\|}{\boldsymbol{\lambda}_{\min}(\boldsymbol{W})}. \tag{32}$$

In this case, $\dot{\boldsymbol{V}}_1 \le 0$, $\boldsymbol{V_1}$ is positive definite matrix, according to the boundedness theorem, when $\boldsymbol{V}(\tilde{\boldsymbol{\zeta}})$ is bounded, $\tilde{\boldsymbol{\zeta}}$ as its domain should also be bounded. As mentioned above, $\boldsymbol{f_1(t)}$ is bounded and differentiable as the "total disturbance", and it can be known from (27), $\dot{\boldsymbol{\zeta}}$ is bounded. From the above analysis of bounded conditions and (32), we can know that $\dot{\boldsymbol{V}}_1$ is bounded. Finally according to Barbalat's lemma, when $t \to \infty$, then $\tilde{\boldsymbol{\zeta}} \to 0$, so the system is Lyapunov asymptotically stable [37].

Similarly, the closed-loop controller of the jib is proved to be asymptotically stable, that is, $\dot{\boldsymbol{V}}_2 \le 0$, then $\dot{\boldsymbol{V}} = \dot{\boldsymbol{V}}_1 + \dot{\boldsymbol{V}}_2 \le 0$.

According to the above analysis and conclusions, the proof of the proposed controller stability analysis can

be accomplished by using LaSalle's invariance principle [38].

4. SIMULATION RESULTS AND DISCUSSION

In this section, we use MATLAB&Simulink to build a mathematical model of the double-pendulum of the tower crane. The parameters of tower crane with double-pendulum are shown in Table 1. Then, the effectiveness and robust performance of the proposed controller is verified by a series of simulations. Firstly, an LQR, a sliding mode controller (SMC), and a partial enhanced-coupling nonlinear controller with initial saturation (PENCIS) [29] are compared to the proposed controller. Then, considering model in different load mass and rope lengths, and external disturbances, we verified the robustness of the proposed controller.

4.1. Simulation conditions

The controller parameters for the double-pendulum tower crane are obtained through careful tuning and are given as follows:

Trolly subcontroller:

$$\begin{aligned} &r_1 = 2.82,\ h_1 = 0.01,\ \omega_1 = 11.9,\ b_1 = 36.23,\\ &k_1 = 0.10,\ k_2 = 2500,\ k_3 = 0.50,\\ &k_4 = 0.10,\ k_5 = 9.90,\ k_6 = 0.01. \end{aligned} \tag{33}$$

Jib subcontroller:

$$\begin{aligned} &r_2 = 2.21,\ h_2 = 0.01,\ \omega_2 = 2.88,\ b_2 = 4.81,\\ &k_7 = 0.10,\ k_8 = 0.60,\ k_9 = 0.01,\\ &k_{10} = 0.10,\ k_{11} = 0.10,\ k_{12} = 0.01. \end{aligned} \tag{34}$$

And for the $kas(e,\gamma,\delta)$, their nonlinear parameters are pre-given and generic, therefore we chose the following value for them:

$$\delta = 0.01,\ \gamma_1 = 0.75,\ \gamma_2 = 1.25,\ \gamma_{01} = 1,\ \gamma_{02} = 0.5. \tag{35}$$

4.2. Comparative simulations

For the sake of verifying the superiority of the proposed controller, it is compared with a SMC, a LQR and a PENCIS in simulations.

The nonlinear SMC can be introduced from the linearized matrix (17), and it is that

$$\boldsymbol{S} = \boldsymbol{q_1} + \boldsymbol{\Lambda}(\boldsymbol{q} - \boldsymbol{q_d}),$$

Table 1. Tower crane model.

M_t	5.6 kg	m_1	5 kg	m_2	5 kg
J_0	6.8 kg·m^2	l_1	1 m	l_2	2.5 m
g	9.8 m/s^2	x_d	0.6 m	α_d	30 m

$$\boldsymbol{\Lambda} = diag\{\chi_1\ \chi_2\ \chi_3\ \chi_4\ \chi_5\ \chi_6\}. \tag{36}$$

Set $\boldsymbol{\chi_i}$, $(i = 1, ..., 6)$ are positive elements, then the sliding mode convergence law can be defined as

$$\dot{\boldsymbol{S}} = -\boldsymbol{\mu S} - \boldsymbol{\eta}\tanh(\boldsymbol{S}). \tag{37}$$

In summary, the specific expression of SMC is as follows:

$$U_a = \left(\boldsymbol{b^T b}\right)^{-1}\left(\boldsymbol{b^T}\left(\boldsymbol{d} + \boldsymbol{\Lambda q_1} - \boldsymbol{\mu S} - \boldsymbol{\eta}\tanh(\boldsymbol{S})\right)\right). \tag{38}$$

The LQR controller of linearized tower crane model is designed as follows:

$$\begin{aligned} T_a = &-\vartheta_{11}e_1 - \vartheta_{12}\dot{e}_1 - \vartheta_{13}\theta_2 - \vartheta_{14}\dot{\theta}_2\\ &- \vartheta_{15}\theta_4 - \vartheta_{16}\dot{\theta}_4 + T_f, \end{aligned} \tag{39}$$

$$\begin{aligned} F_x = &-\vartheta_{21}e_2 - \vartheta_{22}\dot{e}_2 - k_{23}\theta_1 - \vartheta_{24}\dot{\theta}_1\\ &- \vartheta_{25}\theta_3 - \vartheta_{26}\dot{\theta}_3 + F_f, \end{aligned} \tag{40}$$

and the $\boldsymbol{Q}$ and $\boldsymbol{R}$ matrices were set as $\boldsymbol{Q} = diag(40, 40, 40, 40, 40, 1, 1, 1, 1, 1, 1)$ and $\boldsymbol{R} = [1\ \ 1]$ to achieve control object, where the controller gains $\vartheta_{11} = 6.32$, $\vartheta_{12} = 12.54$, $\vartheta_{13} = 0.09$, $\vartheta_{14} = 3.25$, $\vartheta_{15} = 1.17$, $\vartheta_{16} = 4.78$, $\vartheta_{21} = 6.32$, $\vartheta_{22} = 13.89$, $\vartheta_{23} = 1.68$, $\vartheta_{24} = 6.55$, $\vartheta_{25} = 2.39$, $\vartheta_{14} = 7.94$.

The PENCIS proposed in [29] is as follows:

$$\begin{aligned} T_\alpha = &-k_{tp}\tanh\left(e_{\varpi_1}\right) - k_{td}\tanh\left(\dot{e}_{\varpi_1}\right)\\ &- \varepsilon_1\kappa_1\left(\lambda_1\dot{\theta}_2 + \dot{\theta}_4\right) + T_f, \end{aligned} \tag{41}$$

$$\begin{aligned} F_x = &-k_{fp}\tanh\left(e_{\varpi_2}\right) - k_{fd}\tanh\left(\dot{e}_{\varpi_2}\right)\\ &- \varepsilon_2\kappa_2\left(\lambda_2\dot{\theta}_1 + \dot{\theta}_3\right) + F_f, \end{aligned} \tag{42}$$

where $k_{tp} = 15.00$, $k_{td} = 21.00$, $k_{fp} = 16.00$, $k_{fd} = 32.00$ are gain factors. The above T_f and T_f are defined in (7) and (8). $e_{\varpi_1} = \varpi_1 - \alpha_d$, $e_{\varpi_2} = \varpi_2 - x_d$, $\dot{e}_{\varpi_1} = \dot{\varpi}_1$, $\dot{e}_{\varpi_2} = \dot{\varpi}_2$, and the expressions for ϖ_1 and ϖ_2 are as follows:

$$\varpi_1 = \alpha + \mu_{11}\theta_2 + \mu_{12}\theta_4 + \kappa_1\int_0^t(\lambda_1\theta_2 + \theta_4)\,d\tau, \tag{43}$$

$$\varpi_2 = x + \mu_{21}\theta_1 + \mu_{22}\theta_3 + \kappa_2\int_0^t(\lambda_2\theta_1 + \theta_3)\,d\tau, \tag{44}$$

where $\kappa_1 = -0.25$, $\kappa_2 = -3.50$, $\mu_{11} = -0.40$, $\mu_{12} = -0.50$, $\mu 21 = -0.72$, $\mu_{22} - 0.90$

Firstly, the comparative simulation results were included by Fig. 4, which contains the trolley and jib positioning state information α and x, the hook swing angles θ_1 and θ_2, load swing angles θ_3 and θ_4. Moreover, we also listed significant control indicator data in Table 2 as a quantitative comparative analysis to report the superior control performance of the proposed controller.

It is obviously seen from the figure that the proposed controller can quickly position and eliminate the swing of

Table 2. Quantified analysis results.

Control method	Reaching time t_{xr} (s)	Reaching time $t_{\alpha r}$ (s)	Maximum value θ_{1max} (deg)
Proposed	6.87	6.05	0.35
PENCIS	5.92	4.41	0.92
SMC	6.73	7.22	3.22
LQR	10.29	6.45	1.60
	Maximum value θ_{2max} (deg)	Maximum value θ_{3max} (deg)	Maximum value θ_{4max} (deg)
Proposed	0.43	0.44	0.49
PENCIS	0.55	1.24	0.48
SMC	1.00	3.83	1.47
LQR	0.72	1.94	0.83

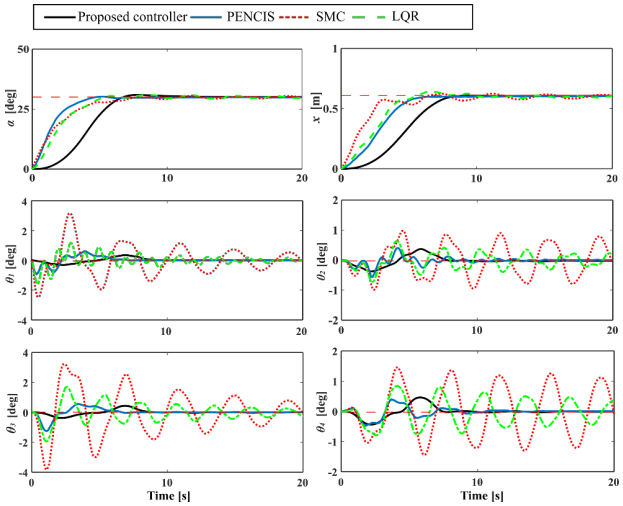

Fig. 4. Comparative simulation results.

the double-pendulum effect. As shown in the figure and table, both SMC and LQR controllers fail to position the jib and trolley in a short time, and their responses exhibit a large overshoot. Meanwhile, the compared controllers can not effectively eliminate the maximum swing angles and then produce serious residual swings. As for the PENCIS, it has better positioning and anti-swing performance than the above controllers, but we think there is still room for suppressing all levels of swing angles. At the same time, the steady-state characteristics are relatively satisfactory but still cannot suppress the "chattering" after eliminating the maximum swing angles. The weakness is that "chattering" phenomenon may increase the energy consumption of the actuator, or induce tower resonance in severe cases.

As shown in Table 2, four performance indicators are utilised as criteria for evaluating the pros and cons of the controllers, that is, $t_{\alpha r}$ (s) and t_{xr} (s) are the attaining time of jib and trolley, and θ_{imax} (deg) is the maximum value of θ_i, $(i = 1, 2, 3, 4)$.The proposed controller can position the jib and the trolley in 6.05 s and 6.87 s, respectively, which are 1.17 s and 3.42 s shorter than the maximum reaching time. Moreover, the swing angles quantization amplitude presented by the proposed controller is 0.35 deg, 0.43 deg, 0.44 deg and 0.49 deg, respectively. And all swing angle values are almost minimum compared to other controllers, and there is decreased by about 81%, 43%, 82%, and 47% respectively compared with the average value of other controllers. From the details of Fig. 4, the proposed controller can effectively suppress the "chattering" after eliminating the swing angles of all levels. To summarize, the quantitative data shows that the proposed controller can not only position the jib/trolley efficiently but also has the best anti-sway control performance among all controllers mentioned.

4.3. Robust performance

In this part, three simulations in different aspects were conducted to verify the robustness performance of the proposed controller when model parameters uncertained and external disturbances. Firstly, considering the uncertainty of the model parameters, we changed the mass of the load and the length of the rope (m_2, l_1) with still using controller gains in (33) and (34). As shown in Fig. 5, Change 50% of the load mass on the basis of 5 kg, that is, 2.5 kg

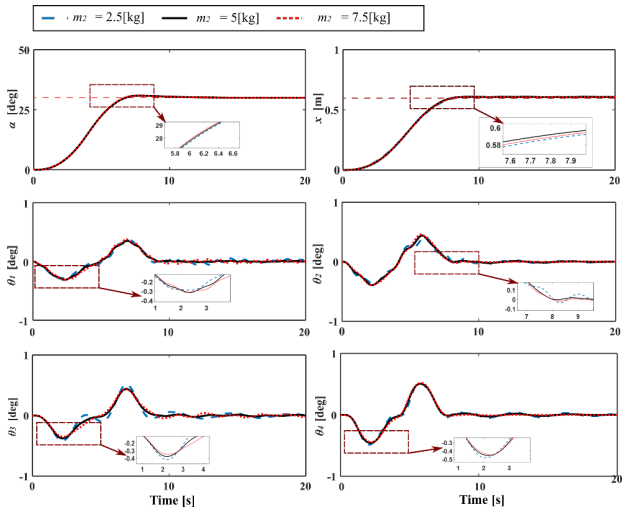

Fig. 5. Simulation results with different load mass.

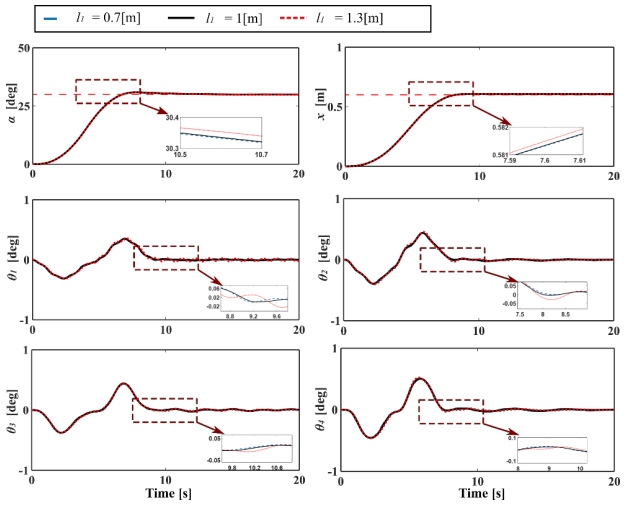

Fig. 6. Simulation results with different rope length.

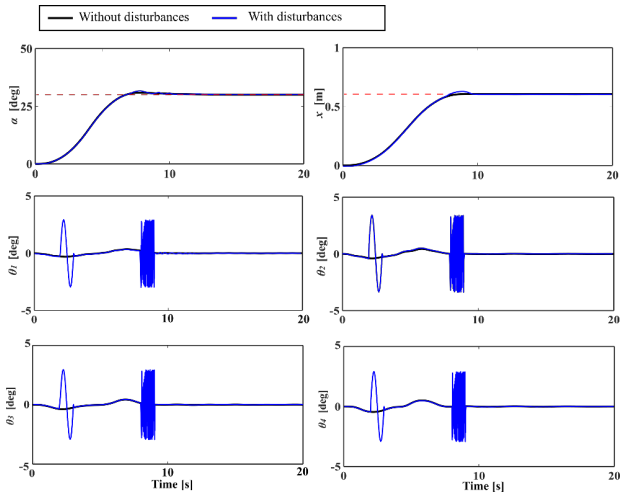

Fig. 7. Simulation results with external disturbances.

and 7.5 kg. And controller performance has not deteriorated. Similarly, the rope length was changed from 0.7 m to 1.3 m, still no obvious interference to the system, the results are obtained in Fig. 6. To sum up, when the model parameters are uncertained, the proposed controller still maintains remarkable control performance and has robustness.

Next, we added continuous white Gaussian noise with power 10^{-8} to simulate actual sensor noise and assess the proposed controller's resistance to external disturbances. We also introduced a sinusoid signal between 2 s and 3 s and a random signal between 8 s and 9 s with a maximum amplitude of 3 deg as swing angle disturbances. The results are shown in Fig. 7. From the figure, the state variables of the system are oscillating during suffering external disturbances, but the system can still converge the state variables immediately after the disturbances without losing the ability of positioning and anti-swing.

5. CONCLUSION

An improved Active Disturbance Rejection Controller with a new nonlinear function was proposed, which achieves robust control for tower crane with double-pendulum effect. In particular, the jib/trolley can eliminate tracking errors quickly and restrain double-pendulum swings effectively. This study presents the first time to address anti-swing and positioning with "chattering" problems for double-pendulum tower crane based on ADRC. Moreover, the proposed controller can perform well in scenes with model parameters uncertained and external disturbances. Hurwitz Criterion, Lyapunov technique, and LaSalle's invariance theorem were utilized to prove the closed-loop system is asymptotically stable. Eventually, a series of comparative simulations are provided to indicate the significant controller performance and strong robustness. In the future, time-varying rope lengths tower crane controller with an algorithm to optimize its gains will be properly designed.

APPENDIX A: THE DETAILED TERMS OF (17)

$$\boldsymbol{U_a} = \begin{bmatrix} T_\alpha & F_x \end{bmatrix}^T,$$

$$\boldsymbol{q_1} = \begin{bmatrix} \alpha & x & \theta_1 & \theta_2 & \theta_3 & \theta_4 \end{bmatrix},$$

$$\boldsymbol{f(t)} = \begin{bmatrix} d_1 & d_2 & d_3 & d_4 & d_5 & d_6 \end{bmatrix},$$

$$\boldsymbol{b} = \begin{bmatrix} b_{11} & b_{21} & b_{31} & b_{41} & b_{51} & b_{61} \\ b_{12} & b_{22} & b_{32} & b_{42} & b_{52} & b_{62} \end{bmatrix}^T,$$

$$b_{11} = \frac{1}{M_t x_d + J_0},\ b_{12} = b_{21} = 0,\ b_{22} = \frac{1}{M_t},$$

$$b_{31} = 0,\ b_{32} = -\frac{1}{M_1 l_1},\ b_{41} = -\frac{x_d}{M_t l_1 {x_d}^2 + J_0 l_1},$$

$$b_{42} = b_{51} = b_{52} = b_{51} = b_{62} = 0,$$

$$d_1 = \frac{(m_1 + m_2)\, g x_d \theta_2}{M_t x_d^2 + J_0},\ d_2 = \frac{(m_1 + m_2 g \theta_1)}{M_t},$$

$$d_3 = \frac{((M_t + m_1)(m_1 + m_2)\,\theta_1 - M_t m_2 \theta_3)\, g}{M_t m_1 l_1},$$

$$d_4 = -\frac{\left(\left(M_t x_d^2 + J_0 + m_1 x_d^2\right)(m_1 + m_2)\,\theta_2 - \left(M_t x_d^2 + J_0\right) m_2 \theta_4\right) g}{m_1 l_1 \left(M_t x_d^2 + J_0\right)},$$

$$d_5 = \frac{(m_1 + m_2)(\theta_1 - \theta_3)\, g}{m_1 l_2},$$

$$d_6 = \frac{(m_1 + m_2)(\theta_2 - \theta_4)\, g}{m_1 l_2}.$$

CONFLICT OF INTEREST STATEMENT

The authors declare that they have no conflict of interest.

REFERENCES

[1] M. Zhang, Y. Zhang, B. Ji, C. Ma, and X. Cheng, "Modeling and energy-based sway reduction control for tower crane systems with double-pendulum and spherical-pendulum effects," *Measurement and Control*, vol. 53, no. 1-2, pp. 141-150, 2020.

[2] D. Blackburn, W. Singhose, J. Kitchen, V. Patrangenaru, J. Lawrence, T. Kamoi, and A. Taura, "Command shaping for nonlinear crane dynamics," *Journal of Vibration and Control*, vol. 16, no. 4, pp. 477-501, 2010.

[3] J. Huang, E. Maleki, and W. Singhose, "Dynamics and swing control of mobile boom cranes subject to wind disturbances," *IET Control Theory & Applications*, vol. 7, no. 9, pp. 1187-1195, 2013.

[4] J. Vaughan, D. Kim, and W. Singhose, "Control of tower cranes with double-pendulum payload dynamics," *IEEE Transactions on Control Systems Technology*, vol. 18, no. 6, pp. 1345-1358, 2010.

[5] N. Sun, Y. Fang, X. Zhang, and Y. Yuan, "Transportation task-oriented trajectory planning for underactuated overhead cranes using geometric analysis," *IET Control Theory & Applications*, vol. 6, no. 10, pp. 1410-1423, 2012.

[6] W. Devesse, M. Ramteen, L. Feng, and J. Wikander, "A real-time optimal control method for swing-free tower crane motions," *Proc. of IEEE International Conference on Automation Science and Engineering (CASE)*, IEEE, pp. 336-341, 2013.

[7] N. Sun, Y. Fang, H. Chen, B. Lu, and Y. Fu, "Slew/translation positioning and swing suppression for 4-dof tower cranes with parametric uncertainties: Design and hardware experimentation," *IEEE Transactions on Industrial Electronics*, vol. 63, no. 10, pp. 6407-6418, 2016.

[8] H. Chen and N. Sun, "Nonlinear control of underactuated systems subject to both actuated and unactuated state constraints with experimental verification," *IEEE Transactions on Industrial Electronics*, vol. 67, no. 9, pp. 7702-7714, 2019.

[9] M. Böck and A. Kugi, "Real-time nonlinear model predictive path-following control of a laboratory tower crane," *IEEE Transactions on Control Systems Technology*, vol. 22, no. 4, pp. 1461-1473, 2013.

[10] Š. Ileš, J. Matuško, and F. Kolonić, "Sequential distributed predictive control of a 3d tower crane," *Control Engineering Practice*, vol. 79, pp. 22-35, 2018.

[11] M. Zhang, Y. Zhang, B. Ji, C. Ma, and X. Cheng, "Adaptive sway reduction for tower crane systems with varying cable lengths," *Automation in Construction*, vol. 119, 103342, 2020.

[12] H. Chen, Y. Fang, and N. Sun, "A swing constraint guaranteed mpc algorithm for underactuated overhead cranes," *IEEE/ASME Transactions on Mechatronics*, vol. 21, no. 5, pp. 2543-2555, 2016.

[13] A. T. Le and S.-G. Lee, "3d cooperative control of tower cranes using robust adaptive techniques," *Journal of the Franklin Institute*, vol. 354, no. 18, pp. 8333-8357, 2017.

[14] N. Sun, Y. Fang, H. Chen, and B. He, "Adaptive nonlinear crane control with load hoisting/lowering and unknown parameters: Design and experiments," *IEEE/ASME Transactions on Mechatronics*, vol. 20, no. 5, pp. 2107-2119, 2014.

[15] W. He, S. Zhang, and S. S. Ge, "Adaptive control of a flexible crane system with the boundary output constraint," *IEEE Transactions on Industrial Electronics*, vol. 61, no. 8, pp. 4126-4133, 2013.

[16] X.-Z. Jin, W.-W. Che, Z.-G. Wu, and H. Wang, "Analog control circuit designs for a class of continuous-time adaptive fault-tolerant control systems," *IEEE Transactions on Cybernetics*, vol. 52, no. 6, pp. 4209-4220, 2022.

[17] H. Chen, Y. Fang, and N. Sun, "An adaptive tracking control method with swing suppression for 4-dof tower crane systems," *Mechanical Systems and Signal Processing*, vol. 123, pp. 426-442, 2019.

[18] L. A. Tuan and S.-G. Lee, "Sliding mode controls of double-pendulum crane systems," *Journal of Mechanical Science and Technology*, vol. 27, no. 6, pp. 1863-1873, 2013.

[19] L. A. Tuan, H. M. Cuong, P. V. Trieu, L. C. Nho, V. D. Thuan, and L. V. Anh, "Adaptive neural network sliding mode control of shipboard container cranes considering actuator backlash," *Mechanical Systems and Signal Processing*, vol. 112, pp. 233-250, 2018.

[20] M.-S. Park, D. Chwa, and M. Eom, "Adaptive sliding-mode antisway control of uncertain overhead cranes with high-speed hoisting motion," *IEEE Transactions on Fuzzy Systems*, vol. 22, no. 5, pp. 1262-1271, 2014.

[21] Z. Liu, N. Sun, Y. Wu, X. Xin, and Y. Fang, "Nonlinear sliding mode tracking control of underactuated tower cranes," *International Journal of Control, Automation, and Systems*, vol. 19, no. 2, pp. 1065-1077, 2021.

[22] T.-S. Wu, M. Karkoub, W.-S. Yu, C.-T. Chen, M.-G. Her, and K.-W. Wu, "Anti-sway tracking control of tower cranes with delayed uncertainty using a robust adaptive fuzzy control," *Fuzzy Sets and Systems*, vol. 290, pp. 118-137, 2016.

[23] D. Qian, S. Tong, and S. Lee, "Fuzzy-logic-based control of payloads subjected to double-pendulum motion in overhead cranes," *Automation in Construction*, vol. 65, pp. 133-143, 2016.

[24] X. Wu, K. Xu, and X. He, "Disturbance-observer-based nonlinear control for overhead cranes subject to uncertain disturbances," *Mechanical Systems and Signal Processing*, vol. 139, p. 106631, 2020.

[25] L.-H. Lee, P.-H. Huang, Y.-C. Shih, T.-C. Chiang, and C.-Y. Chang, "Parallel neural network combined with sliding mode control in overhead crane control system," *Journal of Vibration and Control*, vol. 20, no. 5, pp. 749-760, 2014.

[26] Y. Zhao and H. Gao, "Fuzzy-model-based control of an overhead crane with input delay and actuator saturation," *IEEE Transactions on Fuzzy Systems*, vol. 20, no. 1, pp. 181-186, 2011.

[27] L. Chai, Q. Guo, H. Liu, and M. Ding, "Linear active disturbance rejection control for double-pendulum overhead cranes," *IEEE Access*, vol. 9, pp. 52225-52237, 2021.

[28] H. Ouyang, Z. Tian, L. Yu, and G. Zhang, "Load swing rejection for double-pendulum tower cranes using energy-shaping-based control with actuator output limitation," *ISA Transactions*, vol. 101, pp. 246-255, 2020.

[29] Z. Tian, L. Yu, H. Ouyang, and G. Zhang, "Transportation and swing reduction for double-pendulum tower cranes using partial enhanced-coupling nonlinear controller with initial saturation," *ISA Transactions*, vol. 112, pp. 122-136, 2021.

[30] H. Ouyang, Z. Tian, L. Yu, and G. Zhang, "Adaptive tracking controller design for double-pendulum tower cranes," *Mechanism and Machine Theory*, vol. 153, 103980, 2020.

[31] X. Jin, S. Lü, and J. Yu, "Adaptive NN-based consensus for a class of nonlinear multiagent systems with actuator faults and faulty networks," *IEEE Transactions on Neural Networks and Learning Systems*, vol. 33, no. 8, pp. 3474-3486, 2022.

[32] M. Zhang and X. Jing, "Adaptive neural network tracking control for double-pendulum tower crane systems with nonideal inputs," *IEEE Transactions on Systems, Man, and Cybernetics: Systems*, vol. 52, no. 4, pp. 2514-2530, 2022.

[33] H. Ouyang, Z. Tian, L. Yu, and G. Zhang, "Partial enhanced-coupling control approach for trajectory tracking and swing rejection in tower cranes with double-pendulum effect," *Mechanical Systems and Signal Processing*, vol. 156, 107613, 2021.

[34] B.-Z. Guo and H.-C. Zhou, "The active disturbance rejection control to stabilization for multi-dimensional wave equation with boundary control matched disturbance," *IEEE Transactions on Automatic Control*, vol. 60, no. 1, pp. 143-157, 2014.

[35] X.-H. Chang, J. Song, and X. Zhao, "Fuzzy Resilient h∞ filter design for continuous-time nonlinear systems," *IEEE Transactions on Fuzzy Systems*, vol 30, no. 2, pp. 591-596, 2022.

[36] Z. Gao, "Scaling and bandwidth-parameterization based controller tuning," *Proc. of the American Control Conference*, vol. 6, pp. 4989-4996, 2006.

[37] X.-H. Chang and Y. Liu, "Quantized output feedback control of AFS for electric vehicles with transmission delay and data dropouts," *IEEE Transactions on Intelligent Transportation Systems*, vol. 23, no. 9, pp. 16026-16037, 2022.

[38] H. K. Khalil, *Nonlinear Systems*, 3rd ed., Patience Hall, vol. 115, 2002.

Xinyu Kang received his B.Eng. degree from the Southwest Minzu University, Chengdu, China, in 2020, where he is currently pursuing an M.S. degree with the College of Information Science and Engineering, Wuhan University of Science and Technology, Wuhan, China. His research interests include the nonlinear control of underactuated system.

Lin Chai received his M.Eng. and Ph.D. degrees from the Wuhan University of Science and Technology, Wuhan, China, in 2005 and 2019, respectively. Since 2005, he has been with the College of Information Science and Engineering, Wuhan University of Science and Technology, where he is currently a Professor. He has published more than ten papers in journals and international conferences. His major research interests include under-actuated system control, industrial network control, power systems, and its automation.

Huikang Liu received his M.Eng. degree from the Wuhan University of Science and Technology, Wuhan, China, in 1988. Since 1988, he has been with the College of Information Science and Engineering, Wuhan University of Science and Technology, where he is currently a Professor. His major research interests include intelligent equipment, new electric drive, and equipment fault diagnosis.